

International Journal of Pattern Recognition and Artificial Intelligence
© World Scientific Publishing Company

6D Object Pose Estimation Based on 2D Bounding Box

Jin Liu

*LIESMARS, Wuhan University
Wuhan, Hubei, China
41038331@qq.com*

Sheng He

*LIESMARS, Wuhan University
Wuhan, Hubei, China
whusheng1996@163.com*

In this paper, we present a simple but powerful method to tackle the problem of estimating the 6D pose of objects from a single RGB image. Our system trains a novel convolutional neural network to regress the unit quaternion, which represents the 3D rotation, from the partial image inside the bounding box returned by 2D detection systems. Then we propose an algorithm we call Bounding Box Equation to efficiently and accurately obtain the 3D translation, using 3D rotation and 2D bounding box. Considering that the quadratic sum of the quaternions four elements equals to one, we add a normalization layer to keep the networks output on the unit sphere and put forward a special loss function for unit quaternion regression. We evaluate our method on the LineMod dataset and experiment shows that our approach outperforms base-line and some state of the art methods.

Keywords: 6D pose estimation; convolutional neural network; Bounding Box Equation.

1. Introduction

Object detection and localization has always been a hot topic of computer vision. Traditional methods like YOLO[1], SSD[2], and so on, have experienced a tremendous success in 2D domain. However, they cant achieve accurate semantic understanding of the objective three-dimensional world, for there is no information about the rotation and position between the object and the camera. A pose of a rigid object has 6 degrees of freedom, 3 in translation and 3 in rotation, and its full knowledge is required in many robotic and scene understanding applications[3]. Recently, much attention has been paid to 6D pose estimation. However, estimating the 6D pose of an object is a huge challenge due to various factors, such as the different shapes and visual angles, lighting conditions and occlusions between objects.

Currently, feature-based methods[4,5,6], template-based methods[7,8] and RGB-D methods[9,10,11,12,13] have achieved robust results to some extent. Feature-based methods tackled this task by matching feature points between 3D mod-

els and images. However, only when there are rich textures on the objects that those methods work. As a result, they are unable to handle texture-less objects[14]. Template-based methods use a rigid template to match different locations in the input image. Such methods are likely to be affected by occlusions. RGB-D methods use depth data as additional information, which simplifies the task. However, active depth sensors are power hungry, which makes 6D objective detection methods for passive RGB images more attractive for mobile and wearable cameras[15]. Besides, acquiring depth data needs additional hardware costs.

Deep learning techniques have recently become mainstream to estimate 6D object pose. In this paper, we propose a generic framework which overcomes the shortcomings of existing methods to estimate 6D object pose. We introduce a brand new method to estimate the 3D rotation \mathbf{R} and the 3D translation \mathbf{T} from a single RGB image. The key idea of our method is to leverage the results returned by current robust 2D detection systems to recover the 6D pose of objects. Our frame divides the pose estimation task into two main stages. In the first stage, we resize the 2D bounding box returned by a 2D detection system and feed it into a novel convolutional neural network (we call the network Q-Net) to regress the 3D rotation \mathbf{R} . In the second stage, our algorithm, Bounding Box Equation, figures out the 3D translation \mathbf{T} using \mathbf{R} produced in the former stage and the position information of the 2D bounding box on the original image. We choose the unit quaternion \mathbf{q} as our 3D rotation representation. The unit quaternion \mathbf{q} is a vector of unit length, so the output of the network should be a unit vector, too. Therefore, to enhance the unit quaternion regression, we add a normalization layer to keep the networks output on the unit sphere, and propose a special loss function, Dot Product Loss, for networks whose outputs require to be unit vectors.

We evaluate our method on the LineMod dataset[17], a benchmark for 6D pose estimation. Experiment shows that on this challenging dataset, our Q-Net and Bounding Box Equation work efficiently and productively, while achieving state-of-the-art results regardless of the complex scenes in the pictures. Additionally, we use our method to detect the 6D pose of common objects in daily life, and the result is also pretty satisfying. In summary, our work has the following advantages and contributions:

1. Our method doesnt need any depth data and works on both texture and texture-less images. And it has practical value and can be applied in daily life.
2. Our method can easily work with current robust 2D detection systems.
3. We propose a novel convolutional neural network for 3D rotation regression named Q-Net and develop a special loss function, Dot Product Loss, for networks whose outputs require to be unit vectors.
4. We introduce Bounding Box Equation, a new algorithm to obtain 3D translation using \mathbf{R} and 2D bounding box in an efficient and accurate manner.

The remainder of the paper is organized as follows. After the overview of related work, we introduce our approach for 6D object pose estimation. Then we display the experimental results, followed by the final conclusion.

2. Related Work

In this section, we review existing techniques designed for 6D pose estimation ranging from traditional approaches to current methods.

Traditional approaches. Feature-based methods and template-based methods are the most traditional techniques in this field. Feature-based methods extract local features described with local descriptors from points of interest in the image, then match them to features on the 3D models to recover the 6D poses[4,5,6,18,19]. For instance, [18] uses SIFT descriptors and clustered images from similar viewpoints into a single model. [19] presents a fast and scalable perception system for object recognition and pose estimation. However, those methods suffer from a common limitation that they require sufficient textures on the objects. To deal with insufficient texture objects, feature learning approaches[17,20] are proposed and outperforms matching approaches. But the basic design of them is time-consuming and multi-stage. In template-based methods[7,8], a rigid template is scanned across the image, and a distance measure is computed to find the best match. These methods can work accurately and quickly, but perform poorly when dealing with clutter and occlusions.

RGB-D approaches. Depth cameras make RGB-D object pose estimation methods[9,10,11,12,13,21,22,23] prevalent. For example, Brachmann et al. proposed an algorithms suitable for generic objects, both textured and texture-less[9]. Sock et al. proposed a multi-view framework to recognize 6DOF pose of multiple object instances in a crowded scene[21]. Zach et al. developed a dynamic and fast method for RGB-D images. The task can be simplified by using depth images, but acquiring depth data takes extra hardware costs.

CNN-based approaches. In recent years, CNN has become the mainstream to solve 6D pose problems, including camera pose[24, 25] and object pose[26,16,27,28,15,29]. Both [24] and [25] train CNNs to directly regress 6D camera pose. Camera pose estimation is much easier for there is no need to detect any object. In [24] the authors use quaternion as rotation representation but omit the spherical constraint, using an unreasonable loss function. [25] addresses the problem by developing a more scientific loss function.

In [26,16], the authors use CNNs to regress 3D object pose directly, their works focus only on 3D rotation estimation while 3D translation is not included. In [27], SSD detection framework[2] is extended to 6D pose estimation. The authors transform pose detection into two-stage classification tasks, view angle classification and in-plane rotation classification. However, wrong classification in either stage could cause an incorrect pose estimation. In BB8[28], the authors firstly use a segmentation network to localize objects. Then another CNN is used to predict the 2D projections of the 3D bounding boxes corners around the object. The 6D pose is estimated through a PnP algorithm. Finally, a CNN is trained to refine the pose. BB8 achieves high precision but is too time-consuming. Similar to BB8, [15] extends YOLO object detection framework[1] to predict the 2D projections of the corners

of the 3D bounding box, then employs PnP algorithm to get the 6D pose. Both [28] and [15] regress too much 2D points, which actually increases the learning difficulty and slows the learning speed. Unlike those mentioned above, Mousavian et al. first use a CNN to regress 3D object orientation, then combines these estimates with geometric constraints provided by a 2D object bounding box to produce a complete 3D bounding box[29]. However, in general, this method needs to solve 4096 linear equations. In special circumstances, such as the KITTI dataset[30], object pitch and roll angles are both zero, there are still 64 equations to be solve, which makes the method computational costly. Our method avoids those problems mentioned above.

3. Approach

In this section, we will describe our approach towards 6D object pose estimation.

3.1. Overall Framework

The overall pipeline of our approach is shown in Fig. 1. Given a RGB image, we firstly leverage a robust 2D object detection algorithm to locate the object and obtain the 2D bounding box, which is resized to 48*48 and input into Q-Net to regress the unit quaternion \mathbf{q} . Then we convert \mathbf{q} to rotation matrix \mathbf{R} and employ Bounding Box Equation to figure out the 3D translation \mathbf{T} . Finally, we project the eight corners of the 3D bounding box onto the image to visualize the 3D rotation and translation.

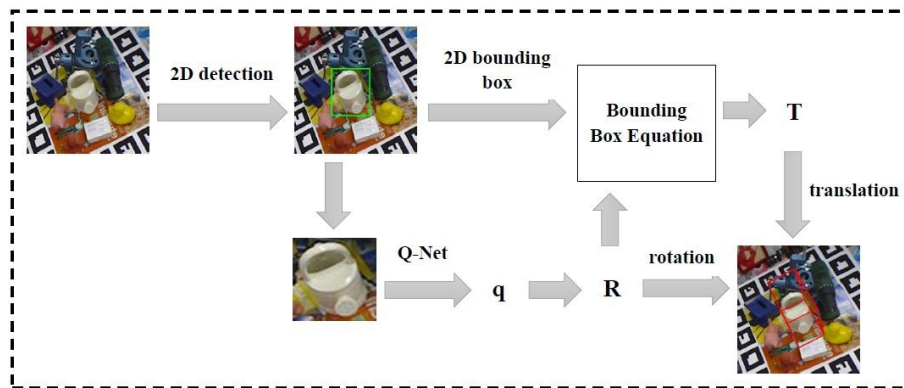


Fig. 1. Pipeline of our method.

3.2. Q-Net Architecture

Euler angles, rotation matrix and unit quaternion are three main representations of 3D rotation. Euler angles are easily understandable as they describe three angles of rotation about three axes. However, regressing Euler angles directly can be a hard work due to multiple problems. For example, poses that are very similar visually might be far away in Euler angle space[16]. Rotation matrix is an orthogonal matrix with 3*3 elements and has many special properties. However, regressing it is inappropriate for it is difficult to enforce the orthogonality constraint when learning a 3D rotation representation through back-propagation[25].

Compared to the former two representations, unit quaternion is much more suitable. So to avoid those problems caused by Euler angles and rotation matrix, we choose unit quaternion, $\mathbf{q} = (q_0, q_1, q_2, q_3)$ as the representation. The only one problem with unit quaternion is that \mathbf{q} and $-\mathbf{q}$ represent the same rotation. For the loss layer, \mathbf{q} and $-\mathbf{q}$ will produce the maximum error, which will make the prediction unstable. To address the problem, we constrain all quaternions to one hemisphere. We define \mathbf{q}_+ to represent the unit quaternion whose first element is larger than zero. If $q_0 < 0$, we change the quaternion to \mathbf{q}_+ .

$$q_+ = \begin{cases} q, & q_0 > 0 \\ -q, & q_0 \leq 0 \end{cases} \quad (1)$$

To regress unit quaternion, we developed the CNN, Q-Net. The architecture is shown in Fig. 2.

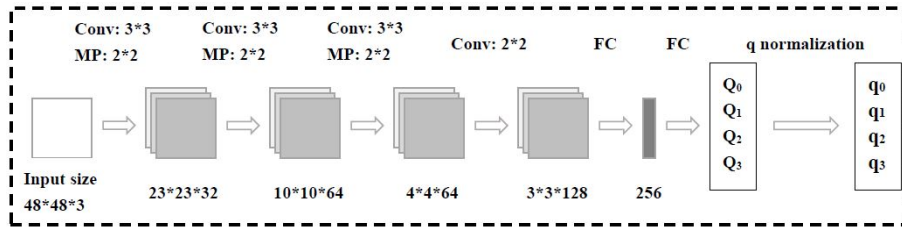


Fig. 2. The architecture of Q-Net. Conv means convolution, MP means max pooling, and FC means fully connected. The step size of convolution and max pooling is 1 and 2, respectively.

Unit quaternion meets the constraint condition:

$$q_0^2 + q_1^2 + q_2^2 + q_3^2 = 1 \quad (2)$$

However, the fully connected layer doesn't guarantee that the network output a unit vector. So like [16], we add an additional layer, q normalization layer, to keep

the output on the unit sphere. In q normalization layer, the forward-propagation is as follows:

$$q_i = \frac{Q_i}{\sqrt{Q_0^2 + Q_1^2 + Q_2^2 + Q_3^2}}, i = 0, 1, 2, 3 \quad (3)$$

where Q_i is the output of the last fully connected, and q_i is the output of q normalization layer.

In [16], the authors have proven that the normalization layer helps improve the accuracy of prediction. Actually, q normalization layer can also accelerate the training of the network. We trained two networks, one with q normalization and the other without that. Apart from the normalization, the two network share the same structure, initialization and samples. We found that with q normalization the loss converged much faster and the training performance is much better, as is shown in Fig. 3.

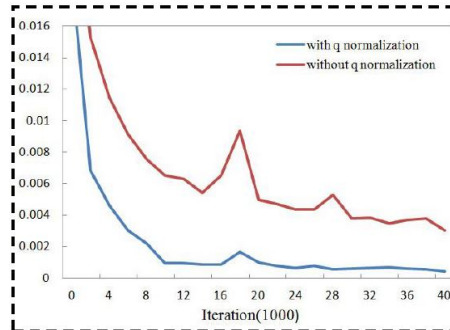


Fig. 3. The convergence of the loss. The ordinate axis represents the value of the loss, and the abscissa axis represents the iteration.

3.3. Dot Product Loss

We regard the learning of unit quaternion as a regression problem. Due to the special property of unit quaternion, the networks output should be a unit vector. To this end, we propose a novel loss function, Dot Product Loss, for networks whose output requires to meet unit constraint. The loss function is defined as follows:

$$L_{dot} = \frac{1}{2} (1 - \hat{q} \cdot q) \quad (4)$$

where q is the output of network, and \hat{q} is the ground-truth.

For two unit vectors, their dot product is never larger than one.

$$\hat{q} \cdot q = \cos(\theta) \leq 1 \quad (5)$$

Only when the two vectors are exactly the same that their dot product equals to one. Under the circumstances, Dot Product Loss reaches the minimum value zero. The neural network reduces the loss through continuous iteration optimization, meanwhile makes the output and ground-truth closer and closer.

When used in regressing unit quaternion, Dot Product Loss is as follows:

$$L_{dot} = \frac{1}{2} \left(1 - \sum_{i=0}^3 \hat{q}_i q_i \right) \quad (6)$$

Both \hat{q} and q are on the four dimensional sphere. Fig. 4 describes the geometric meaning of Dot Product Loss.

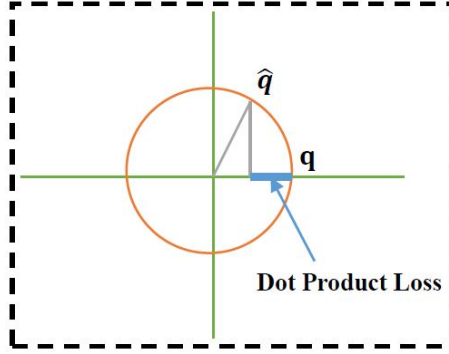


Fig. 4. The geometric meaning of Dot Product Loss. The red circle refers to the four dimensional sphere.

The backward propagation of q normalization layer is as follows:

$$\frac{\partial L_{dot}}{\partial Q_i} = \sum_{j=0}^3 \frac{\partial L_{dot}}{\partial \hat{q}_j} \times \frac{\partial \hat{q}_j}{\partial Q_i} = \sum_{j=0}^3 \left(-\frac{1}{2} q_j \right) \times \frac{\partial \hat{q}_j}{\partial Q_i} = -\frac{1}{2} \sum_{j=0}^3 q_j \times \frac{\partial \hat{q}_j}{\partial Q_i} \quad (7)$$

where

$$\begin{cases} \frac{\partial \hat{q}_j}{\partial Q_i} = \frac{1}{A} \left(1 - \frac{Q_i^2}{A^2} \right) = \frac{1}{A} (1 - \hat{q}_i^2) & i = j \\ \frac{\partial \hat{q}_j}{\partial Q_i} = \frac{-Q_i Q_j}{A^3} = \frac{-\hat{q}_i \hat{q}_j}{A} & i \neq j \\ A = \sqrt{Q_0^2 + Q_1^2 + Q_2^2 + Q_3^2} \end{cases} \quad (8)$$

3.4. Bounding Box Equation

Bounding Box Equation can figure out 3D translation efficiently and accurately, leveraging 3D rotation produced by Q-Net and the 2D bounding box on the original image. The core idea is to use point-to-side correspondence constraint to calculate 3D translation \mathbf{T} . The algorithm consists of two step.

Step 1 Finding out the four point-to-side correspondence constraints.

There are n points on the surface of the object, we name them P_1, P_2, \dots, P_n . Assuming that the origin of the object coordinate frame is in the inside of the object, and the 3D coordinates of those points are $X_1=[x_1, y_1, z_1]^T, X_2=[x_2, y_2, z_2]^T, \dots, X_n=[x_n, y_n, z_n]^T$. This step is to find out which four points on the surface are corresponding to the four sides of 2D box, as is shown in Fig. 5. Here we introduce two approach.



Fig. 5. The point-to-side correspondence. The surface of the object consists of quantities of points. Here we assume that P_1, P_2, P_3 and P_4 touch the four sides.

Approach 1 Indirect comparison. According to perspective projection,

$$z \begin{bmatrix} u \\ v \\ 1 \end{bmatrix} = KR(X - T) \quad (9)$$

where K is the camera matrix, R is the rotation matrix, u and v are the pixel coordinate, z is the objects z -coordinate in the camera coordinate frame and has no impact on the point-to-side correspondence, and it is a positive number. Firstly, we take 2D boxes center (u_0, v_0) and the origin of the object coordinate frame, $X_0 = (0, 0, 0)^T$ and a positive number, for example $z = 100$, into equation (9).

$$z \begin{bmatrix} u_0 \\ v_0 \\ 1 \end{bmatrix} = KR(X_0 - T) \quad (10)$$

We get

$$T_0 = -z(KR)^{-1} \begin{bmatrix} u_0 \\ v_0 \\ 1 \end{bmatrix} \quad (11)$$

T_0 is not the real 3D translation, but it helps find out the point-to-side correspondence. And we take z , T_0 into equation (9) to get equation (12).

$$z \begin{bmatrix} u \\ v \\ 1 \end{bmatrix} = KR(X - T_0) \quad (12)$$

Then we take the n points 3D coordinates into equation (12) and compute n pairs of pixels coordinates, (u_1, v_1) , (u_2, v_2) , ..., (u_n, v_n) . Among those we find the maximum u , v and minimum u , v . The point results in maximum u is corresponding to the right side of the 2D box, we record its index and name it iR . Similarly, the point results in minimum u touches the left side, we record its index and name it iL . The point results in maximum v touches the bottom side, we record its index and name it iB . The point results in minimum v touches the up side, we record its index and name it iT . Up to now we find out which four points are corresponding to the four sides of 2D box.

Approach 2 Direct conversion. For the n points on the surface,

$$z_i \begin{bmatrix} u_i \\ v_i \\ 1 \end{bmatrix} = KR(X_i - T_0) \quad (13)$$

Taking (11) into (13),

$$z_i \begin{bmatrix} u_i \\ v_i \\ 1 \end{bmatrix} = KR \left(X_i + z(KR)^{-1} \begin{bmatrix} u_0 \\ v_0 \\ 1 \end{bmatrix} \right) = KRX_i + z \begin{bmatrix} u_0 \\ v_0 \\ 1 \end{bmatrix} \quad (14)$$

Establishing a coordinate frame whose origin is at the objects center, and the three axis are corresponding to the camera's three axis respectively. According to the coordinate transformation principle, in this coordinate frame, the coordinates of point P_i is $RX_i = [\Delta X_i, \Delta Y_i, \Delta Z_i]$. And we get

$$KRX_i = \begin{bmatrix} f_x \Delta X_i + c_x \Delta Z_i \\ f_y \Delta Y_i + c_y \Delta Z_i \\ \Delta Z_i \end{bmatrix} = \begin{bmatrix} P_{xi} \\ P_{yi} \\ \Delta Z_i \end{bmatrix} \quad (15)$$

where f_x, f_y, c_x, c_y are the elements of camera matrix. z is the objects z -coordinate in the camera coordinate frame and is much larger than ΔZ_i . so,

$$\frac{\Delta Z_i}{z} \approx 0 \quad (16)$$

From (14), (15) and (16) we get

$$\begin{cases} u_i = \frac{f_x \Delta X_i + c_x \Delta Z_i + z u_0}{\Delta Z_i + z} = \frac{\frac{f_x \Delta X_i}{z} + \frac{c_x \Delta Z_i}{z} + u_0}{\frac{\Delta Z_i}{z} + 1} \approx \frac{f_x \Delta X_i}{z} + u_0 \\ v_i = \frac{f_y \Delta Y_i + c_y \Delta Z_i + z v_0}{\Delta Z_i + z} = \frac{\frac{f_y \Delta Y_i}{z} + \frac{c_y \Delta Z_i}{z} + v_0}{\frac{\Delta Z_i}{z} + 1} \approx \frac{f_y \Delta Y_i}{z} + v_0 \end{cases} \quad (17)$$

From (17) we can see that the values of u_i and v_i are determined by ΔX_i and ΔY_i if we assign a positive number to z . (15) can simplify to

$$RX_i = \begin{bmatrix} \Delta X_i \\ \Delta Y_i \\ \Delta Z_i \end{bmatrix} \quad (18)$$

We take n points' 3D coordinates into (18) and calculate n pair of $[\Delta X, \Delta Y, \Delta Z]$, through which we can infer which four points result in the maximum and minimum u, v . And we find out the four points corresponding to the four sides of 2D bounding box.

Step 2 Figuring out 3D translation

In the former step, we find out the four points and name their indexes iL, iR, iT and iB . According to collinearity equation,

$$\begin{cases} u_{Ki} = \frac{u_i - c_x}{f} = \frac{r_{11}(x_i - t_x) + r_{12}(y_i - t_y) + r_{13}(z_i - t_z)}{r_{31}(x_i - t_x) + r_{32}(y_i - t_y) + r_{33}(z_i - t_z)} \\ v_{Ki} = \frac{v_i - c_y}{f} = \frac{r_{21}(x_i - t_x) + r_{22}(y_i - t_y) + r_{23}(z_i - t_z)}{r_{31}(x_i - t_x) + r_{32}(y_i - t_y) + r_{33}(z_i - t_z)} \end{cases} \quad (19)$$

where (t_x, t_y, t_z) is the elements of T and unknown, T is the cameras 3D coordinate in the object coordinate frame. (x_i, y_i, z_i) is the 3D coordinate. We linearize (19) and get

$$\begin{cases} (u_{Ki}r_{31} - r_{11})t_x + (u_{Ki}r_{32} - r_{12})t_y + (u_{Ki}r_{33} - r_{13})t_z = \\ (u_{Ki}r_{31} - r_{11})x_i + (u_{Ki}r_{32} - r_{12})y_i + (u_{Ki}r_{33} - r_{13})z_i \\ (v_{Ki}r_{31} - r_{21})t_x + (v_{Ki}r_{32} - r_{22})t_y + (v_{Ki}r_{33} - r_{23})t_z = \\ (v_{Ki}r_{31} - r_{21})x_i + (v_{Ki}r_{32} - r_{22})y_i + (v_{Ki}r_{33} - r_{23})z_i \end{cases} \quad (20)$$

According to the four point-to-side correspondence constraints, we get

$$\begin{cases} (u_{KiL}r_{31} - r_{11})t_x + (u_{KiL}r_{32} - r_{12})t_y + (u_{KiL}r_{33} - r_{13})t_z = \\ (u_{KiL}r_{31} - r_{11})x_{iL} + (u_{KiL}r_{32} - r_{12})y_{iL} + (u_{KiL}r_{33} - r_{13})z_{iL} \\ (u_{KiR}r_{31} - r_{11})t_x + (u_{KiR}r_{32} - r_{12})t_y + (u_{KiR}r_{33} - r_{13})t_z = \\ (u_{KiR}r_{31} - r_{11})x_{iR} + (u_{KiR}r_{32} - r_{12})y_{iR} + (u_{KiR}r_{33} - r_{13})z_{iR} \\ (v_{KiT}r_{31} - r_{21})t_x + (v_{KiT}r_{32} - r_{22})t_y + (v_{KiT}r_{33} - r_{23})t_z = \\ (v_{KiT}r_{31} - r_{21})x_{iT} + (v_{KiT}r_{32} - r_{22})y_{iT} + (v_{KiT}r_{33} - r_{23})z_{iT} \\ (v_{KiB}r_{31} - r_{21})t_x + (v_{KiB}r_{32} - r_{22})t_y + (v_{KiB}r_{33} - r_{23})t_z = \\ (v_{KiB}r_{31} - r_{21})x_{iB} + (v_{KiB}r_{32} - r_{22})y_{iB} + (v_{KiB}r_{33} - r_{23})z_{iB} \end{cases} \quad (21)$$

(21) can be written in matrix form as follows:

$$AT = X_{box} \quad (22)$$

where

$$A = \begin{bmatrix} u_{KiL}r_{31} - r_{11} & u_{KiL}r_{32} - r_{12} & u_{KiL}r_{33} - r_{13} \\ u_{KiR}r_{31} - r_{11} & u_{KiR}r_{32} - r_{12} & u_{KiR}r_{33} - r_{13} \\ v_{KiT}r_{31} - r_{21} & v_{KiT}r_{32} - r_{22} & v_{KiT}r_{33} - r_{23} \\ v_{KiB}r_{31} - r_{21} & v_{KiB}r_{32} - r_{22} & v_{KiB}r_{33} - r_{23} \end{bmatrix} = \begin{bmatrix} b_{Left} \\ b_{Right} \\ b_{Top} \\ b_{Bottom} \end{bmatrix} \quad (23)$$

We call equation (22) Bounding Box Equation, the matrix A Bounding Box Matrix, and the four row vectors Side Vector. In (23),

$$\begin{cases} u_{KiL} = \frac{x_L - c_x}{f_x} \\ u_{KiR} = \frac{x_R - c_x}{f_y} \\ v_{KiT} = \frac{y_T - c_y}{f_x} \\ v_{KiB} = \frac{y_B - c_y}{f_y} \end{cases} \quad (24)$$

where x_L, y_L, x_R, y_R are the pixel coordinates of the 2D bounding boxes borders. In Bounding Box Equation,

$$X_{box} = \begin{bmatrix} (u_{KiL}r_{31} - r_{11})x_{iL} + (u_{KiL}r_{32} - r_{12})y_{iL} + (u_{KiL}r_{33} - r_{13})z_{iL} \\ (u_{KiR}r_{31} - r_{11})x_{iR} + (u_{KiR}r_{32} - r_{12})y_{iR} + (u_{KiR}r_{33} - r_{13})z_{iR} \\ (v_{KiT}r_{31} - r_{21})x_{iT} + (v_{KiT}r_{32} - r_{22})y_{iT} + (v_{KiT}r_{33} - r_{23})z_{iT} \\ (v_{KiB}r_{31} - r_{21})x_{iB} + (v_{KiB}r_{32} - r_{22})y_{iB} + (v_{KiB}r_{33} - r_{23})z_{iB} \end{bmatrix} = \begin{bmatrix} b_{Left} \bullet X_{iL} \\ b_{Right} \bullet X_{iR} \\ b_{Top} \bullet X_{iT} \\ b_{Bottom} \bullet X_{iB} \end{bmatrix} \quad (25)$$

We call the four row vectors Bounding Box Vector. The norm of Side Vector is as follows:

$$\begin{cases} \|b_{Left}\|^2 = \|\{u_{KiL}r_{31} - r_{11}, u_{KiL}r_{32} - r_{12}, u_{KiL}r_{33} - r_{13}\}\|^2 = u_{KiL}^2 + 1 \\ \|b_{Right}\|^2 = \|\{u_{KiR}r_{31} - r_{11}, u_{KiR}r_{32} - r_{12}, u_{KiR}r_{33} - r_{13}\}\|^2 = u_{KiR}^2 + 1 \\ \|b_{Top}\|^2 = \|\{v_{KiT}r_{31} - r_{21}, v_{KiT}r_{32} - r_{22}, v_{KiT}r_{33} - r_{23}\}\|^2 = v_{KiT}^2 + 1 \\ \|b_{Bottom}\|^2 = \|\{v_{KiB}r_{31} - r_{21}, v_{KiB}r_{32} - r_{22}, v_{KiB}r_{33} - r_{23}\}\|^2 = v_{KiB}^2 + 1 \end{cases} \quad (26)$$

To solve Bounding Box Equation, we use least square method.

$$T = (AA^T)^{-1} A^T X_{box} \quad (27)$$

Here, the T we get is the cameras 3D coordinate in the object coordinate frame. 3D translation \mathbf{T} is the objects 3D coordinate in the camera coordinate. \mathbf{T} can be obtained by the follow equation:

$$\mathbf{T} = -RT \quad (28)$$

4. Experiments

In this section, we present and discuss the results of our method.

4.1. Implementation Details

We test our approach both on LineMod dataset[17] and daily objects. For there is only one object of interest on each image, we choose MTCNN[31] as the 2D detection system to obtain the 2D bounding box. Then use Q-Net and Bounding Box Equation to estimate the 6D pose.

We train Q-Net by SGD with momentum, using a mini-batch size of 24 images and variable learning rates, step is the learning rate policy. The step size is set 10^4 and gamma is set 0.8. Other parameters are set as follows: momentum 0.9, weight decay 4×10^{-3} , and base learning rate 10^{-4} . Xavier initialization is chosen for weights and zero-initialize biases. Dropout is included where used behind the full connection layer. All models are trained and tested with Caffe.

4.2. 6D Pose Estimation Results

Fig. 6 and Fig. 7 respectively show the results of 6D pose estimation on LineMod and daily objects. LineMod provides a point cloud for each object, so we use all the 3D coordinates of the point cloud in Bounding Box Equation. Actually, there is no need to use so much points. While testing on the daily objects, no point cloud is provided, we use eight corners to estimate the 3D translation.



Fig. 6. Pose estimation results of our method on LineMod dataset[17]. The blue 3D bounding boxes refer to the ground-truth, and the red refer to the estimation results.

To our knowledge, there is no benchmark for daily objects 6D pose estimation, due to which present methods are confined to the laboratory environment and haven't been widely applied. In our experiments, all the training data of daily objects are annotated by ourselves.

4.3. State Of The Art Comparisons

To evaluate our method and compare it with some state of the art methods, we use two evaluation metrics.

Average Euler angle error. This is a metric appropriate for 3D rotation estimation accuracy evaluation. It is used in [16] and matches the one used in [33]. Both [16] and [33] train CNNs to regress the 3D rotation. Average Euler angle error is the average of the absolute difference in angle (in degrees) between the estimated 3D rotation and the ground truth, measured regarding the three principal axes[16]. Since we use unit quaternion representation, we transform it into Euler angle to perform the comparisons. Table 1 shows the comparisons with [16] and [33].

5cm 5°. This is a metric appropriate for 6D pose estimation accuracy evaluation. As in [34], we use the percentage of correctly predicted poses for each object. With this metric, a pose is considered correct if the translational and rotational error[3] are below 5cm and 5° respectively. The translational error (e_{TE}) and rotational error (e_{RE}) are as follows:

$$e_{TE}(\hat{t}, \bar{t}) = \|\bar{t} - \hat{t}\|_2 \quad (29)$$



Fig. 7. Pose estimation results of our method on daily objects. The first line shows a radio and a cup, the second shows a stool and a book. These pictures are taken by ourselves. The third line shows the results on cars, the pictures are taken from Pascal VOC dataset[32].

Table 1. State of the art comparisons of our method against the one of Wohlhart et al.[33] and Doumanoglou et al.[16] in the LineMod dataset[17]. The former two dont provide results for eggbox and glue, hence for the sake of comparison the average is taken over the first 11 objects.

Object	[33]	[16]	ours
ape	15.0	11.8	5.3
benchviseblue	15.5	13.2	6.1
camera	12.0	10.1	4.8
can	15.5	12.3	4.9
cat	14.0	10.4	4.6
driller	17.8	13.2	5.9
duck	13.9	10.9	5.0
holepuncher	13.2	11.4	5.5
iron	11.4	10.2	6.2
lamp	13.3	11.1	4.2
phone	18.2	11.7	4.8
average	14.53	11.48	5.21
eggbox	-	-	5.1
glue	-	-	5.2

$$e_{RE}(\hat{R}, \bar{R}) = \arccos\left(\left(\text{Tr}\left(\hat{R}\bar{R}^{-1}\right) - 1\right)/2\right) \quad (30)$$

where \hat{R} and \bar{R} are the estimated pose, and \bar{R} are the ground truth pose. The error e_{RE} is given by the angle from the axis-angle representation of rotation[35]. In [34] the authors introduce an approach to estimate 6D pose from a single RGB image. Our method relies on RGB images, too. Table 2 shows the comparisons with [34].

4.4. Computation Times

On LineMod dataset, our implementation takes 16ms for 2D detection (MTCNN), 2ms for 3D rotation prediction, and 1ms for Bounding Box Equation, on a GeForce GTX 1080 GPU.

5. Conclusion

In this work, we propose a method that extracts 6D pose from a single RGB image based on 2D bounding box. This method inherits the previous 2D object detection algorithm very well. On this basis, we train Q-Net on Dot Product Loss to regress the unit quaternion and use Bounding Box Equation to obtain 3D translation. Experiments show that the method is feasible, efficient and practical. Up to now, our method is limited in single type objects pose estimation. As a future work, we would like to further improve the performance and focus on how to extend this

Table 2. State of the art comparisons of our method against the one of Wohlhart et al.[33] and Doumanoglou et al.[16] in the LineMod dataset[17]. The former two dont provide results for eggbox and glue, hence for the sake of comparison the average is taken over the first 11 objects.

Object	[34]	ours
ape	34.4	55.0
benchvisblue	40.6	44.0
camera	30.5	62.5
can	48.4	64.8
cat	34.6	67.7
driller	54.5	50.0
duck	22.0	58.4
eggbox	57.1	60.0
glue	23.6	59.6
holepuncher	47.3	55.6
iron	58.74	46.7
lamp	49.3	70.1
phone	26.8	60.5
average	40.60	58.07

method in order to tackle multi type objects pose estimation. Moreover, we plan to extend the dataset to daily objects.

References

1. J. Redmon, S. Divvala, R. Girshick, and A. Farhadi. You Only Look Once: Unified, Real-Time Object Detection. In *CVPR*, 2016.
2. W. Liu, D. Anguelov, D. Erhan, C. Szegedy, S. Reed, C. Fu, and A. C. Berg. SSD: Single Shot MultiBox Detector. In *ECCV*, 2016.
3. T. Hodan, J. Matas, and S. Obdrzalek. On Evaluation of 6D Object Pose Estimation. In *ECCV*, 2014.
4. A. Collet, M. Martinez, and S. S. Srinivasa. The MOPED framework: Object recognition and pose estimation for manipulation. In *IJRR*, 2011.
5. D. G. Lowe. Object recognition from local scaleinvariant features. In *ICCV*, 1999.
6. F. Rothganger, S. Lazebnik, C. Schmid, and J. Ponce. 3D object modeling and recognition using local affine-invariant image descriptors and multiview spatial constraints. In *IJCV*, 2006.
7. S. Hinterstoisser, C. Cagniart, S. Ilic, P. Sturm, N. Navab, P. Fua, and V. Lepetit. Gradient Response Maps for Real-Time Detection of Texture-less Objects. In *TPAMI*, 2012.
8. S. Hinterstoisser, V. Lepetit, S. Ilic, S. Holzer, G. Bradski, K. Konolige, and N. Navab. Model Based Training, Detection and Pose Estimation of Texture-Less 3D Objects in Heavily Cluttered Scenes. In *ACCV*, 2012.
9. E. Brachmann, A. Krull, F. Michel, S. Gumhold, J. Shotton, and C. Rother. Learning 6D Object Pose Estimation Using 3D Object Coordinates. In *ECCV*, 2014.

10. C. Choi and H. I. Christensen. 3D Textureless Object Detection and Tracking: An Edge-Based Approach. In *IROS*, 2012.
11. C. Choi and H. I. Christensen. RGB-D Object Pose Estimation in Unstructured Environments. In *Robotics and Autonomous Systems*, 2016.
12. W. Kehl, F. Milletari, F. Tombari, S. Ilic, and N. Navab. Deep Learning of Local RGB-D Patches for 3D Object Detection and 6D Pose Estimation. In *ECCV*, 2016.
13. K. Lai, L. Bo, X. Ren, and D. Fox. A Large-Scale Hierarchical Multi-View RGB-D Object Dataset. In *ICRA*, 2011.
14. Y. Xiang, T. Schmidt, V. Narayanan and D. Fox. PoseCNN: A Convolutional Neural Network for 6D Object Pose Estimation in Cluttered Scenes. *arXiv preprint arXiv:1711.00199*, 2017.
15. B. Tekin, S. Sinha, and P. Fua. Real-Time Seamless Single Shot 6D Object Pose Prediction. *arXiv preprint arXiv:1711.08848*, 2017.
16. A. Doumanoglou, V. Balntas, R. Kouskouridas, and T. K. Kim. Siamese Regression Networks with Efficient mid-level Feature Extraction for 3D Object Pose Estimation.. In *NIPS*, 2016.
17. A. Krull, E. Brachmann, F. Michel, M. Y. Yang, S. Gumhold, and C. Rother. Learning analysis-by-synthesis for 6D pose estimation in RGB-D images. In *ICCV*, 2015.
18. D. G. Lowe. Local Feature View Clustering for 3D Object Recognition. In *CVPR*, 2001.
19. M. Martinez, A. Collet, S. S. Srinivasa. MOPED: A Scalable and Low Latency Object Recognition and Pose Estimation System. In *ICRA*, 2010.
20. F. Michel, A. Kirillov, E. Brachmann, A. Krull, S. Gumhold, B. Savchynskyy, and C. Rother. Global hypothesis generation for 6D object pose estimation. In *CVPR*, 2017.
21. J. Sock, S. H. Kasaei, L. S. Lopes, and T.-K. Kim. Multi-view 6D Object Pose Estimation and Camera Motion Planning using RGBD Images. In *ICCV*, 2017.
22. H. Zhang and Q. Cao. Combined Holistic and Local Patches for Recovering 6D Object Pose. In *ICCV*, 2017.
23. C. Zach, A. Penate-Sanchez, and M.-T. Pham. A Dynamic Programming Approach for Fast and Robust Object Pose Recognition from Range Images. In *CVPR*, 2015.
24. A. Kendall, M. Grimes, and R. Cipolla. PoseNet: A convolutional network for real-time 6-dof camera relocalization. In *ICCV*, 2015.
25. A. Kendall and R. Cipolla. Geometric loss functions for camera pose regression with deep learning. In *CVPR*, 2017.
26. S. Mahendran, H. Ali, and R. Vidal. 3D Pose Regression using Convolutional Neural Networks. In *CVPR*, 2017.
27. Wadim Kehl, Fabian Manhardt, Federico Tombari, Slobodan Ilic, and Nassir Navab. SSD-6D: making rgbbased 3D detection and 6D pose estimation great again. In *ICCV*, 2017.
28. M. Rad and V. Lepetit. BB8: A scalable, accurate, robust to partial occlusion method for predicting the 3D poses of challenging objects without using depth. In *ICCV*, 2017.
29. A. Mousavian, D. Anguelov, J. Flynn, and J. Koeck. 3D Bounding Box Estimation using Deep Learning and Geometry. In *CVPR*, 2017.
30. A. Geiger, P. Lenz, C. Stiller, and R. Urtasun. Vision meets robotics: The KITTI dataset. In *IJRR*, 2013.
31. K. Zhang, Z. Zhang, Z. Li, and Y. Qiao. Joint Face Detection and Alignment Using Multitask Cascaded Convolutional Networks. In *IEEE Signal Processing Letters*, 2016.
32. M. Everingham, SMA Eslami, LV Gool, and et al. The Pascal Visual Object Classes Challenge: A Retrospective. In *Lecture Notes in Computer Science*, 2015.
33. P. Wohlhart and V. Lepetit. Learning descriptors for object recognition and 3d pose

- estimation. In *CVPR*, 2015.
34. E. Brachmann, F. Michel, A. Krull, M. M. Yang, S. Gumhold, and C. Rother. Uncertainty-Driven 6D Pose Estimation of Objects and Scenes from a Single RGB Image. In *CVPR*, 2016.
 35. A. Morawiec. Orientations and rotations: computations in crystallographic textures. In *Springer Science & Business Media*, 2004.
-